iScience

CellPress

Article

Wnt-Responsive Stem Cell Fates in the Oral Mucosa

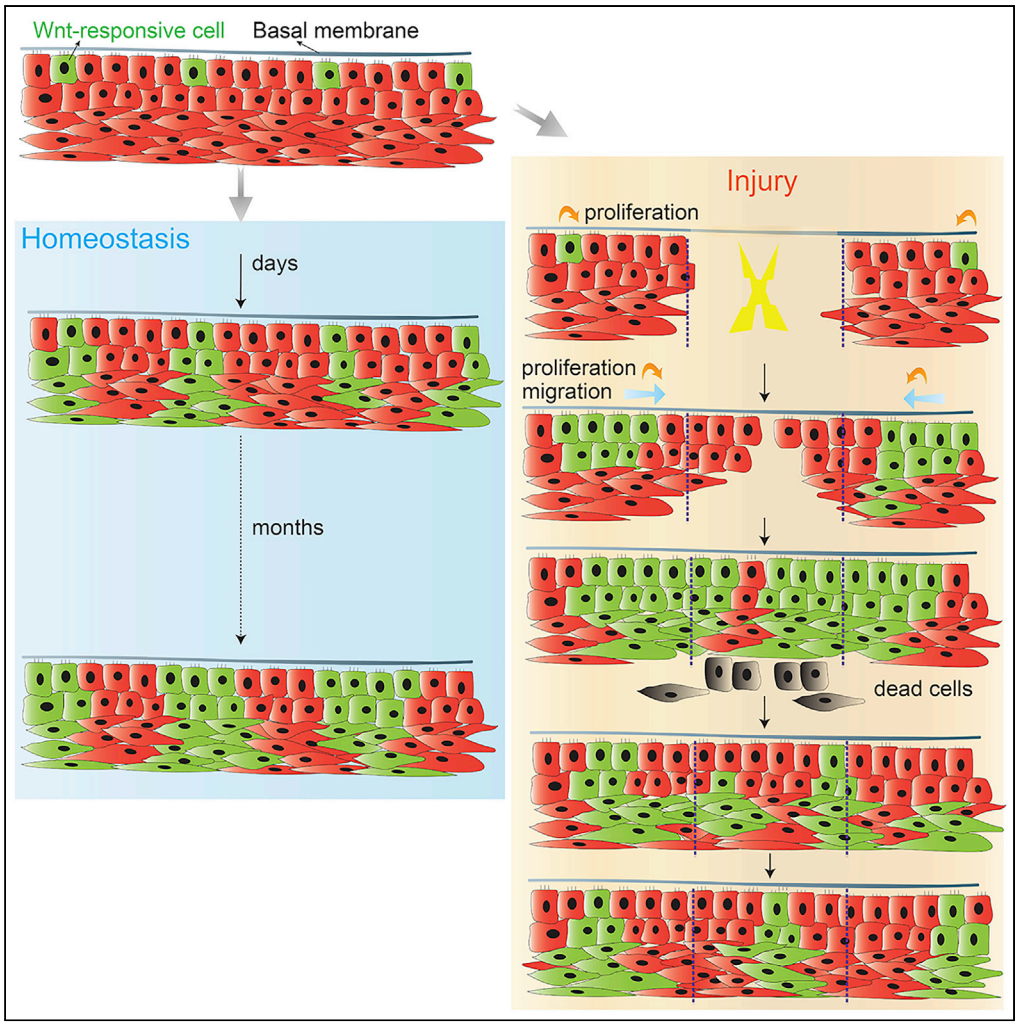

Xue Yuan, Quanchen Xu, Xiaohui Zhang, Lauren A. Van Brunt, Pavla Ticha, Jill A. Helms

xueyuan@stanford.edu (X.Y.)
jhelms@stanford.edu (J.A.H.)

HIGHLIGHTS

During homeostasis, long-lived stem cells in the oral epithelium are Wnt responsive

After injury, the soft palate re-epithelizes faster than the hard palate

Faster healing is attributable to an abundance of Wnt-responsive cells

After healing, the Wnt-responsive stem cell pool returns to homeostatic levels

Yuan et al., iScience *21*, 84–94
November 22, 2019
https://doi.org/10.1016/j.isci.2019.10.016

iScience

CellPress

Article

Wnt-Responsive Stem Cell Fates in the Oral Mucosa

Xue Yuan,[1,*] Quanchen Xu,[1,2] Xiaohui Zhang,[1,3] Lauren A. Van Brunt,[1] Pavla Ticha,[1] and Jill A. Helms[1,4,*]

SUMMARY

Epithelia of the oral cavity exhibit variations in morphologies and turnover rates. Are these differences related to environment or to region-specific stem cell populations? A lineage-tracing strategy allowed visualization of Wnt-responsive cells, and their progeny, in the hard and soft palates. In both anatomic locations, Wnt-responsive basal cells self-renewed and gave rise to supra-basal cells. Palatal injuries triggered an enlargement of this population, and their descendants were responsible for wound re-epithelialization. Compared with the hard palate, soft palate stem cells exhibited an earlier, more robust burst in proliferation, culminating in significantly faster repair. Thereafter, excess Wnt-responsive basal cells were removed, and stem cell numbers were restored back to homeostatic level. Thus, we uncovered a stem cell population in oral mucosa, and its relative abundance is correlate with the rate of oral wound healing. Besides the activation during injury, an endogenous mechanism exists to constrain the stem cell pool after repair.

INTRODUCTION

The mucosal lining of the oral cavity serves as a barrier to protect the underlying tissues from mechanical damage and noxious stimuli. Like other covering and lining tissues of the body, the oral mucosa consists of a surface epithelial layer and a supporting fibrous connective tissue layer (Jones and Klein, 2013; Winning and Townsend, 2000). The connective tissue mainly provides mechanical support and nutrients for the epithelium, whereas the epithelium constantly turns over to protect the underlying connective tissue against mechanical and chemical insults (Squier and Kremer, 2001; Winning and Townsend, 2000).

In mammals, the oral mucosa can be divided into three categories based on function and histology: masticatory mucosa that includes the hard palate and gingiva; lining mucosa that covers the soft palate, the ventral surface of the tongue, as well as buccal, alveolar, and labial surfaces; and specialized mucosa on the dorsal surface of the tongue (Jones and Klein, 2013). Despite distinct functions and morphologies, all oral mucosa is contiguous. Whether they share the same stem cell population and similar remodeling mechanism is largely unknown.

The Wnt pathway is essential for stem cell maintenance and differentiation (Clevers et al., 2014; Kretzschmar and Clevers, 2017; Lien and Fuchs, 2014). The advent of lineage tracing techniques has made it possible to precisely tag populations that arise from Wnt-responsive cells and follow their fate(s) over time. Using Wnt reporters, Wnt responsiveness appears to be a general feature of stem cells in different tissues (Bowman et al., 2013; van Amerongen et al., 2012; Wang et al., 2015). In this study, we used two Wnt reporter strains to specifically visualize Wnt-responsive cells and examine their fates in the oral epithelia, here focusing on the hard and soft palates. Although these two tissues represent two different types of oral mucosa with distinct morphologies, we discovered that they shared a similar homeostatic mechanism. Upon injury, however, the hard and soft palates displayed distinctive, dynamic changes that led to significantly different healing rates. In addition to the critical role of Wnt-responsive cells in turnover and regeneration, we also demonstrated that in oral epithelia the number of Wnt-responsive basal cells is tightly controlled: instead of producing progeny to occupy all layers of the oral epithelia, a large portion of injury-induced progeny remain in the basal layer to cover the injury site; once the tissue has undergone repair, a subset of those labeled basal cells are removed via a non-apoptotic mechanism, which returns the tissue to its initial homeostatic state. These data have implications for improving the repair of slow-to-heal oral injuries.

RESULTS

The Hard and Soft Palates Contain Wnt-Responsive Cells

The hard palate comprises the roof of the oral cavity (Figure 1A) and is characterized by a thick, keratinized epithelium with dense connective tissue underneath (Figure 1B), which makes it an ideal tissue to support

[1]Division of Plastic and Reconstructive Surgery, Department of Surgery, Stanford University School of Medicine, 1651 Page Mill Road, Palo Alto, CA 94304, USA

[2]The Affiliated Hospital of Qingdao University, College of Stomatology, Qingdao University, Qingdao 266003, China

[3]State Key Laboratory of Oral Diseases, National Clinical Research Center for Oral Diseases, West China Hospital of Stomatology, Sichuan University, Chengdu 610041, China

[4]Lead Contact

*Correspondence: xueyuan@stanford.edu (X.Y.), jhelms@stanford.edu (J.A.H.)

https://doi.org/10.1016/j.isci.2019.10.016

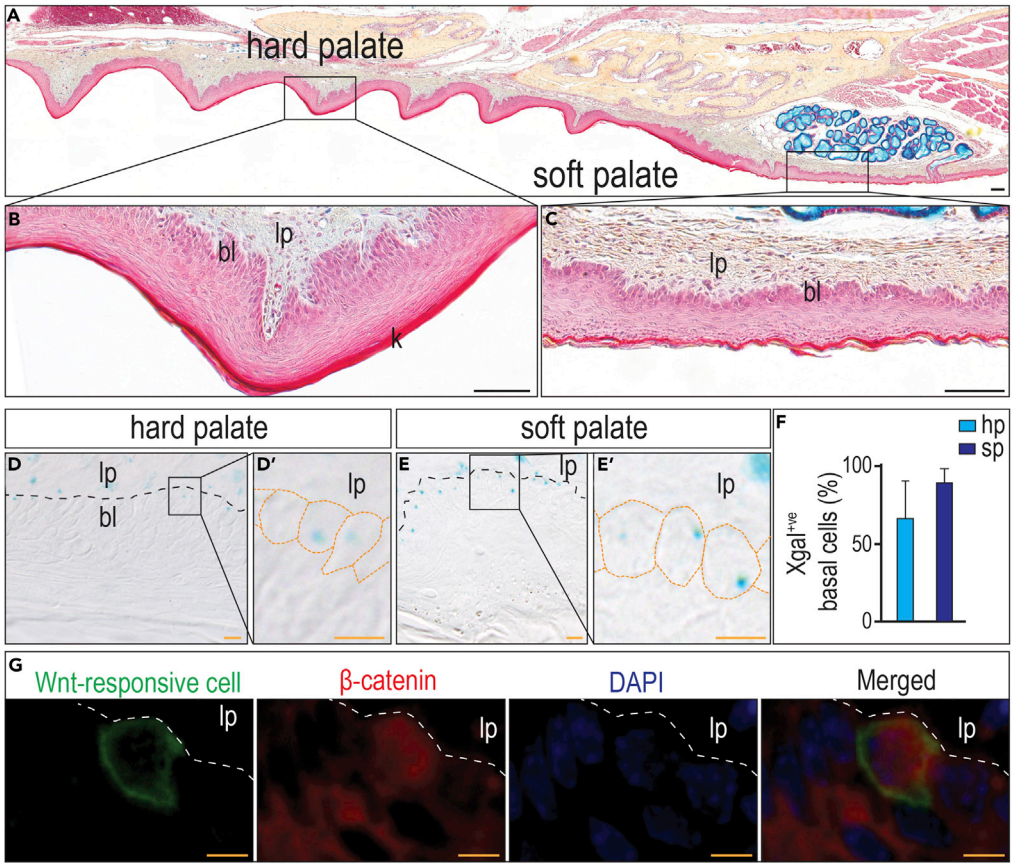

Figure 1. The Hard and Soft Palates Contain Wnt-Responsive Cells

(A–C) (A) Pentachrome staining of the maxilla (sagittal section) showing the different morphology of (B) the hard palate and (C) the soft palate. In pentachrome staining, the epithelial layer stains red and the lamia proper stains yellow to blue. (D–E) In 3-month-old *Axin2*$^{LacZ/+}$ mice, Xgal staining was performed to detect Wnt-responsive cells in (D) the hard palate and (E) the soft palate. The box area in D and E were enlarged in (D′) and (E′). Orange dotted lines indicate the cell shape. (F) Quantification of Xgal^{+ve} basal cells in both hard and soft palates (n = 3, 5 sections per mouse).

(G) Co-staining of GFP^{+ve} cells (tamoxifen was injected 1 day before harvest) with β-catenin (red). The dotted line indicates the basement membrane. Abbreviation: lp, lamia proper; bl, basal layer; hp, hard palate; sp, soft palate; k, keratinized layer. Scale bars: black, 100 μm; orange, 10 μm.

Data represent mean ± SD. See also Figure S1.

mastication. Posteriorly, the hard palate is contiguous with the soft palate (Figure 1A), which has a thin epithelium and loose underlying connective tissue (Figure 1C). This flexible tissue is ideally suited for vocalization. Using an *Axin2*$^{LacZ/+}$ Wnt reporter mouse strain, in which Xgal signal specifically reports Wnt activation in epithelia (Figure S1A), we found Xgal^{+ve}, Wnt-responsive cells in both hard (Figure 1D) and soft palates (Figure 1E). A closer look at the epithelial layers revealed that majority of Xgal^{+ve} Wnt-responsive cells were restricted to the basal layer (Figures 1D′ and 1E′). Basal cells were easy to be recognized by their position, size, and distinctive staining with nuclear fast red (Figure S1B). Quantification of basal cells co-stained with Xgal and nuclear fast red indicated that the soft palate harbored slightly more Wnt-responsive cells than the hard palate (Figure 1F).

Another genetic approach to labeling Wnt-responsive cells, as well as their progeny, involves the use of a *Axin2*$^{CreErt2/+}$; *R26*$^{mTmG/+}$ strain, in which tamoxifen converts Wnt-responsive cells to permanently labeled GFP-expressing cells (van Amerongen et al., 2012).

Based on prior experience (Yuan et al., 2018a, 2018b), a single dose of tamoxifen (5 mg/25 g body weight) resulted in efficient labeling of the palatal epithelium (Figure S2).

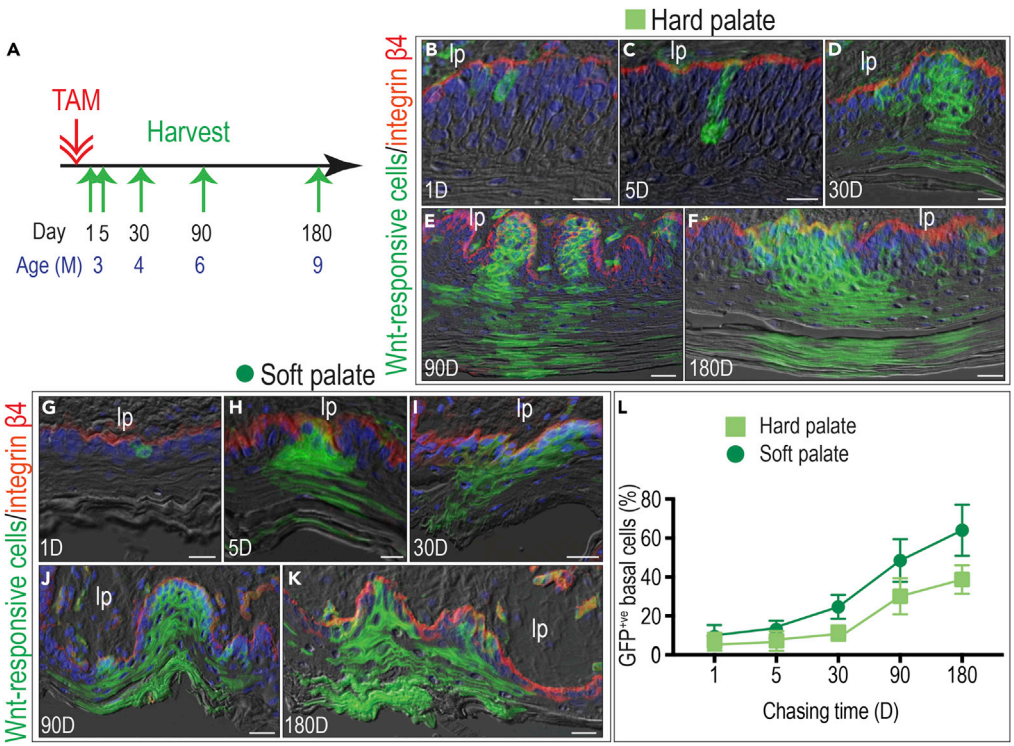

Figure 2. Wnt-Responsive Basal Cells Are Stem Cells in the Hard and Soft Palates

(A) A schematic diagram showing the lineage tracing strategy. Mice were injected with one-dose tamoxifen at the age of 3 months. The Wnt-responsive cells were analyzed 1 day (D), 5D, 30D, 90D, and 180D later.

(B–F) Wnt-responsive cells (green) were co-stained with β4 integrin (red, basement membrane). In the hard palate, (B) 1D chasing showing Wnt-responsive cells close to the basement membrane. These cells (C) expanded within 5D and (D) have established the clone in 30D. (E) 90D later, the clone enlarged and (F) the clone size was maintained in a 180D chasing. In the soft palate.

(G-K) (G) Wnt-responsive cells were first found in the basal layer and (H) the clones were quickly formed within 5D. (I) By 30D, the clone expanded and was maintained through (J) 90D and (K) 180D chasing.

(L) Quantification of GFP^{+ve} basal cells, defined as GFP^{+ve} cells that colocalized with the β4 integrin, in both the hard and soft palates at indicated time points (n = 3, 5 sections for each mouse). Abbreviation: lp, lamia proper. Scale bars: 25 μm. Data represent mean ± SD. See also Figures S2 and S3.

To validate that GFP^{+ve} cells indicated a Wnt-responsive status, tamoxifen was delivered to 3-months-old mice and 1 day later, oral epithelium was analyzed for both GFP and β-catenin (Figure 1G). Co-expression of GFP in cells with evidence of nuclear localization of β-catenin demonstrated that GFP^{+ve} cells were responsive to an endogenous Wnt signal.

Wnt-Responsive Basal Cells Are Stem Cells in Both Hard and Soft Palates

With these tools in hand, we next examined the distribution of Wnt-responsive cells and followed their fates in the hard and soft palates. Tamoxifen was again delivered to 3-month-old-mice (Figure 2A). Within 1 day, analyses of the epithelium of the hard palate showed that GFP^{+ve}, Wnt-responsive cells were primarily anchored to the basement membrane (Figure 2B). By day 5, GFP^{+ve} cell clusters contained both cuboidal basal cells and flattened suprabasal cells (Figure 2C). By day 30, GFP^{+ve} cells formed clones across all layers of the epithelium of the hard palate (Figure 2D). Clones continued to expand and were maintained for at least 180 days (Figures 2E and 2F). In the soft palate, Wnt-responsive cells also represented a subpopulation in the basal layer (Figure 2G). Fate analyses strongly suggested that GFP^{+ve} Wnt-responsive cells were also stem cells (Figures 2H–2K). In terms of absolute number, the soft palate had more Wnt-responsive basal cells than the hard palate (Figure 2L), but in terms of the rate at which these populations grew, they were comparable (Figure S3).

To confirm that Wnt-responsive basal cells were stem cells, hard and soft palate epithelia were harvested, from which single cells were isolated and examined *in vitro* (Figure S4A). First, we confirmed that GFP^{+ve}

cells were basal epithelial cells, by co-immunostaining of GFP (Figure S4B) with keratin 5 (Figure S4C), keratin 14 (Figure S4D), and β4 integrin (Figure S4E). GFP-expressing basal epithelial cells were immune-negative for the suprabasal markers Involucrin (Figure S4F) and loricrin (Figure S4G). The incorporation of EdU suggested that a high percentage of GFP^{+ve} basal cells were proliferative (Figures S4H–S4J). Next, we examined the self-renewing ability of the GFP^{+ve} basal cells using a colony forming unit (CFU) assay. GFP^{+ve} clones were evident after 14 days (Figures S4K and S4L). Taken together, these *in vivo* and *in vitro* data support the conclusion that Wnt-responsive basal cells are stem cells in oral epithelia.

The Soft Palate Displays a Superior Healing Ability Compared with the Hard Palate

A wound in the oral cavity heals faster— and with less scarring—than other epithelial wounds (Iglesias-Bartolome et al., 2018; Politis et al., 2016). The stages of cutaneous wound healing have been well documented (Aragona et al., 2017; Dekoninck and Blanpain, 2019), whereas the same stages of healing in the oral cavity have not. In addition, it is not known whether different types of oral mucosa have different healing abilities. Therefore, we created a 2-mm full-thickness injury at the junction between the hard and soft palates (Figures 3A and 3B). This type of injury allowed us to study healing rates in both tissues. In the soft palate, the wound was clinically healed by post-surgery day (PSD) 3 (Figure 3C). In the hard palate, the injury site was not fully healed until PSD14 (Figures 3D and 3E). Histological analyses verified differences in healing rates. On PSD1, injuries spanning the hard and soft palates had visible wound edges (Figure 3F). By PSD3, the soft palate side of the injury was fully re-epithelialized, but the palate portion of the injury remained open (Figure 3G). By PSD7, the hard palate portion of the injury was re-epithelialized (Figure 3H), but the rugae were not fully reestablished until PSD14 (Figure 3I). Together, these data demonstrated that both hard and soft palates undergo repair in response to injury, but the soft palate does so much faster (Figures 3J and 3K).

Injury in the Soft Palate Induces More Robust Wnt and Proliferation Response

To explore the differential healing mechanisms in these two tissues, we examined the wound edges from the hard (Figure 4A) and soft palates (Figure 4B), focusing on cells that became Wnt responsive as a result of injury using $Axin2^{LacZ/+}$ mice. On PSD3 in the hard palate, $Xgal^{+ve}$, Wnt-responsive cells were abundant, distributed throughout the epithelial layers, and located at a distance (~500 μm) from the wound edge (Figures 4C and 4C′). This represented a departure from the intact state (Figure 4D). In the soft palate, injury also boosted the number of Wnt-responsive cells on PSD3 (Figure 4E), and they were observed in almost all epithelial layers (Figure 4E′; compare with the intact state, Figure 4F). More Wnt-responsive cells were produced in response to soft palate injury versus hard palate injury (compare Figure 4E′ with Figure 4C′).

We next tested whether injury-induced Wnt-responsive cells contributed to tissue repair. On PSD3, the majority of basal cells in the hard palate were proliferating, as indicated by EdU incorporation (Figures 4G and 4G′). This represented a dramatic departure from the intact hard palate, where only ~10% of basal cells were actively proliferating (Figure 4H). In the soft palate, injury also induced a massive cell proliferation (Figures 4I and 4I′). Similar to what we observed in the hard palate, this proliferative burst stood in contrast to the intact state in the soft palate (Figure 4J). The number of proliferating cells was quantified (Figure 4K). Compared with the intact state, injury induced ~5 times more EdU^{+ve} cells in the hard palate and ~11 times more EdU^{+ve} cells in the soft palate (Figure 4K). Collectively, palatal injury stimulated a vigorous Wnt response that was accompanied by a vigorous proliferative response.

Substantial Wnt-Responsive Cells Persist in the Hard Palate after Re-Epithelization

To correlate Wnt-responsive cells with tissue healing, we examined injuries between PSD7 and PSD28. PSD7 was chosen because in the hard palate, the wound was re-epithelialized but not fully regenerated (Figure 5A). In contrast, by PSD7 in the soft palate, the tissue's original architecture was fully restored (Figure 5B). In the hard palate, Wnt-responsive cells were still abundant (Figure 5C). Conversely in the soft palate, the number of Wnt-responsive cells had returned to baseline (Figure 5D).

By PSD14 in the hard palate, the epithelium was thinner (Figure 5E) and rugae were present. The soft palate remained unchanged (Figure 5F). In the hard palate, the population of Wnt-responsive cells remained high in the repaired tissue (Figure 5G). In the soft palate, the number and distribution of Wnt-responsive cells were indistinguishable from that in the intact state (Figure 5H). On PSD28, the number and distribution of $Xgal^{+ve}$ Wnt-responsive cells in the hard palate finally returned to levels seen in the intact state (Figure 5I).

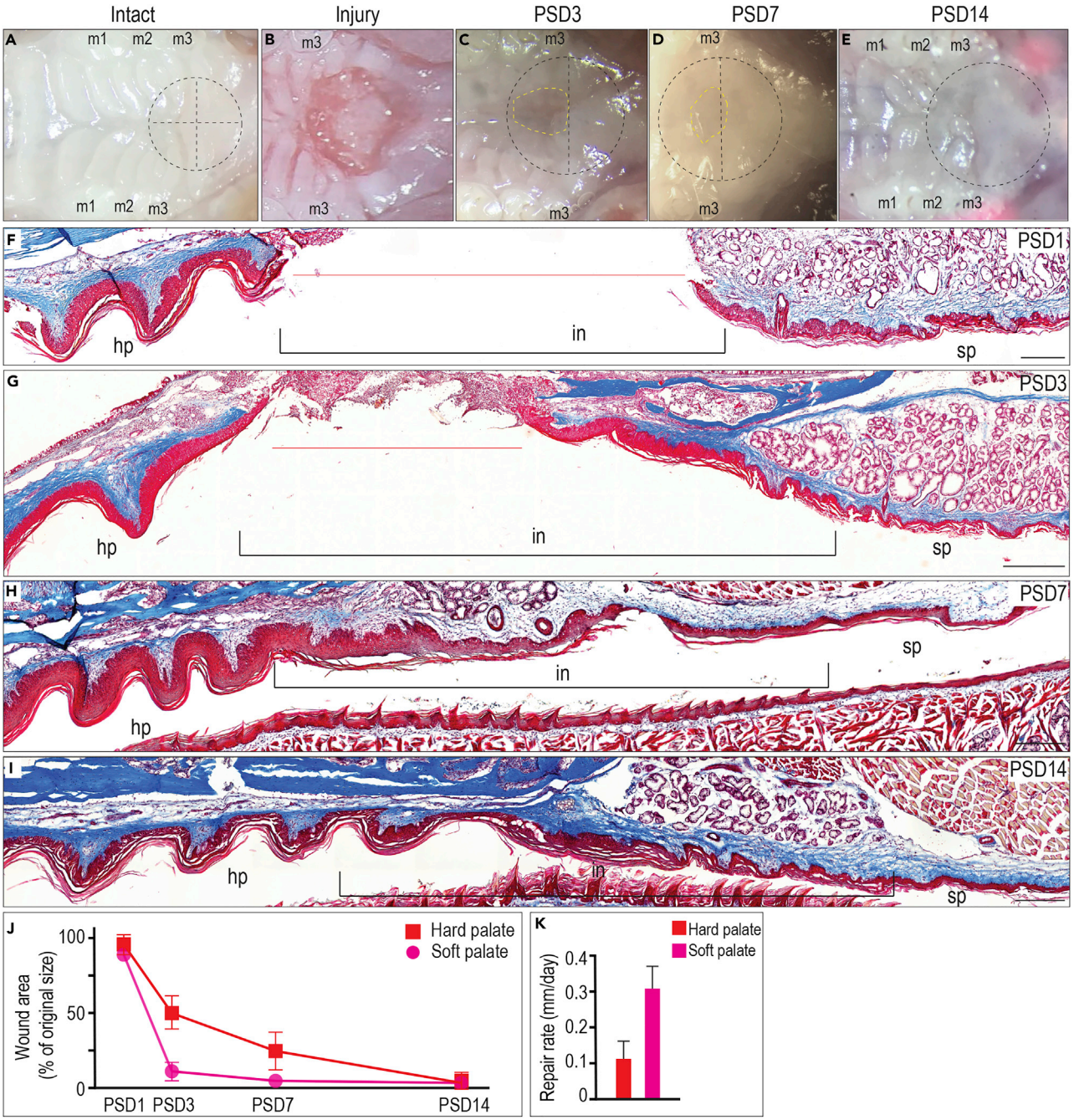

Figure 3. The Soft Palate Displays Superior Healing Ability Than the Hard Palate

(A) Intact hard and soft palates.

(B–E) (B) A 2-mm full-thickness injury (black dashed circle) was created in the area between the hard and soft palates. The center of the injury was located in the cross point of the middle line and the line along with the posterior ends of third molars. Yellow dashed circle indicates the unhealed part. Mice at age of 3 months were subjected to the injury and then monitored for (C) 3 days, (D) 7 days, and (E) 14 days.

(F-I) Representative Masson trichrome staining showing the healing of hard and soft palates on. (F) PSD1, (G) PSD3, (H) PSD7, and (I) PSD14. The black brackets indicate the injury site. The orange lines indicate the unhealed injury.

(J) Quantification of wound area shown in (B)–(E) (n = 6).

(K) Calculated repair rate between PSD1 and PSD3 (n = 6). Abbreviation: m1, maxillary first molar; m2, maxillary second molar; m3, maxillary third molar; PSD, post-surgery day; in, injury; hp, hard palate; sp, soft palate. Data represent mean ± SD. Scale bars: 200 μm.

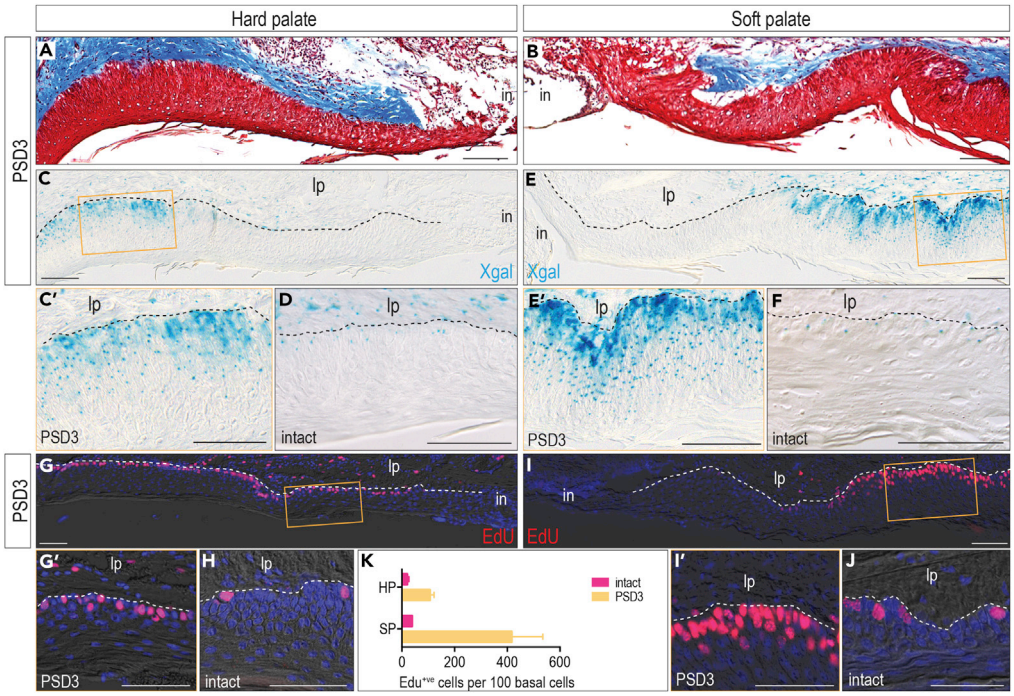

Figure 4. In the Early Stage, Injury Induces More Robust Wnt and Proliferation Response in the Soft Palate

(A–B) On PSD3, representative Masson trichrome staining showing the healing front in (A) the hard palate and (B) the soft palate.

(C-F) In *Axin2*$^{LacZ/+}$ mice, Xgal staining was performed to detect Wnt-responsive cells in (C) the healing hard palate on PSD3 and (D) the intact hard palate. The orange box area in (C) has been enlarged in (C′). Xgal staining was performed to detect Wnt-responsive cells in (E) the healing soft palate on PSD3 and (F) the intact soft palate. The orange box area in (E) has been enlarged in (E′).

(G-I) EdU staining was used to examine cell proliferation in (G) the healing hard palate on PSD3 and (H) the intact hard palate. The orange box area in (G) has been enlarged in (G′). EdU staining was used to examine cell proliferation in (I) the healing soft palate on PSD3 and (J) the intact soft palate. The orange box area in (I) has been enlarged in (I′).

(K) Quantification of EdU^{+ve} cells (n = 6, 5 sections of each mouse). Abbreviation: lp, lamia proper; in, injury; PSD, post-surgery day; hp, hard palate; sp, soft palate. Scale bars: 100 μm.

Data represent mean ± SD. See also Figure S4.

We quantified these changes in the number of Xgal^{+ve} cells over time, and this value was normalized to total basal cell number using nuclear fast red co-staining (Figure S5). In both tissues, Wnt-responsive cells initially escalated in number, followed by their decline over time as the tissue healed. The primary difference between the hard and soft palates was in the magnitude of the response (Figure 5J). In the hard palate, the injury-induced expansion of Wnt-responsive cells was milder and more durable, whereas in the soft palate the increase in Wnt-responsive cells was considerable but transient (Figure 5J). Precisely how this expansion and contraction in Wnt-responsive cells was achieved became the focus of our next experiments.

The Wnt-Responsive Population Enlarges in Response to Injury but Prunes after Homeostasis Is Reestablished

The expansion in Wnt-responsive cells after injury could have been achieved via recruitment of cells. Alternatively, this could reflect the activation of stem cells. To distinguish between these possibilities, we returned to *Axin2*$^{CreErt2/+}$; *R26*$^{mTmG/+}$ strain. Our control group consisted of animals that received tamoxifen but did not sustain any injuries (Figure S6). Our test group consisted of reporter mice that received tamoxifen 2 days before palatal injury (Figure 6A). Cells that are responsive to an endogenous Wnt signal and simultaneously exposed to tamoxifen will stop expressing membrane TdTomato and start expressing membrane GFP (Figure S7). Tamoxifen stops label basal cells 1 day after injection (Figure S2F); therefore, we hypothesized that delivering tamoxifen 2 days before injury would only label resting Wnt-responsive cells in the basal layer and specifically avoid labeling cells that became Wnt-responsive as a result of the

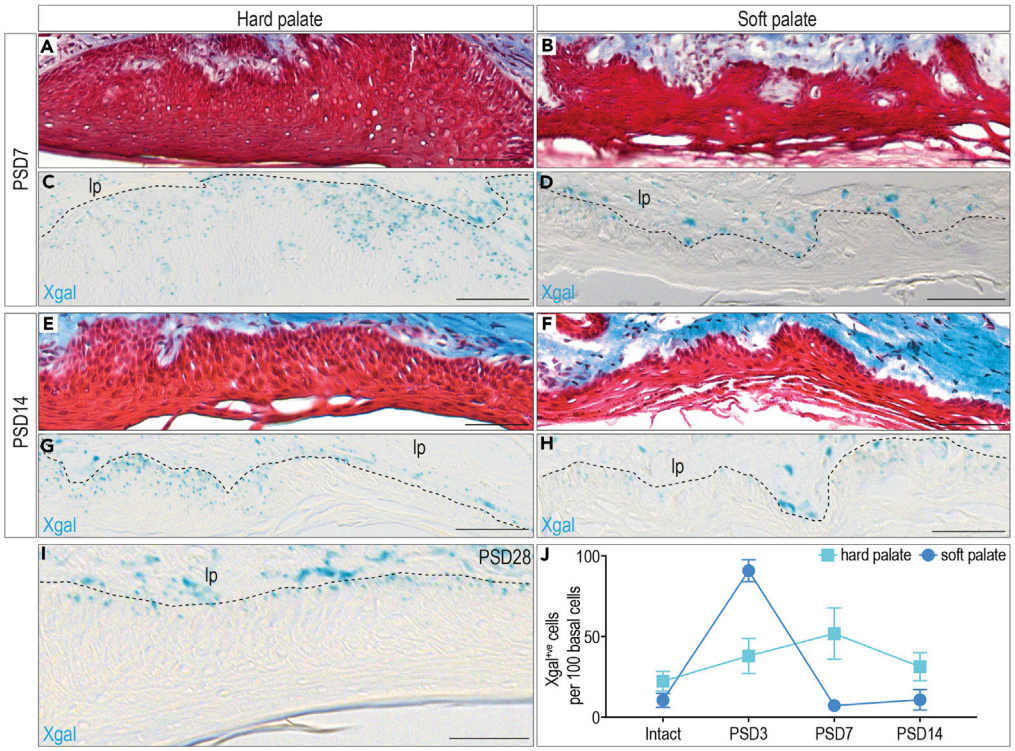

Figure 5. Substantial Wnt-Responsive Cells Persist in the Hard Palate During and Post-Injury Healing

(A–D) Representative Masson trichrome staining showing the healed (A) hard palate and (B) soft palate on PSD7. Xgal staining was performed to detect the Wnt-responsive cells in (C) the healed hard palate and (D) the healed soft palate on PSD7.

(E-H) Representative Masson trichrome staining showing the healed (E) hard palate and (F) soft palate on PSD14. Xgal staining was performed to detect Wnt-responsive cells in (G) the healed hard palate and (H) the healed soft palate on PSD14.

(I) Xgal staining showing Wnt-responsive cells in the healed hard palate on PSD28.

(J) Quantification of $Xgal^{+ve}$ cells in the hard and soft palates at indicated time points (n = 6, 5 sections of each mouse).

Abbreviation: lp, lamia proper; PSD, post-surgery day. Scale bars: 100 μm.

Data represent mean ± SD. See also Figure S4.

tissue damage. Analyses conducted immediately after injury confirmed that the labeling strategy worked: only small clones of GFP^{+ve} cells were in evidence (Figures S6A and S6B), equivalent to the control (intact) group (Figures S6C and S6D).

On PSD3, the GFP^{+ve} population was clustered close to the edge of the injury (Figures S6E and S6F). Compared with the distribution of GFP^{+ve} cells in the intact group (Figures S6G and S6H), there was a dramatic increase in GFP^{+ve} population in injury group (Figures 6B and 6C). Besides the difference in number, suprabasal GFP^{+ve} cells lack the continuity with basal GFP^{+ve} cells during injury, indicating the injury-induced cell migration.

On PSD7, re-epithelialization of the wound was complete and, in this newly formed tissue, progeny of the initial Wnt-responsive stem population had re-established their position in the basal layer and had given rise to much larger clones (compare Figures 6D and 6E with the intact state, Figures S6I and S6J). Given the timing of the labeling (before injury), we conclude that the regenerated tissue arose from the progeny of Wnt-responsive cells residing in the basal layer of the intact palatal epithelia.

In most respects, the hard and soft palates responded similarly to injury, and in both anatomical locations, the Wnt-responsive populations behaved equivalently. What differed significantly, however, was the timing of events: in the hard palate, Wnt-responsive descendants persisted until PSD14 (Figure 6F), but in the soft palate, the GFP^{+ve} population had declined by nearly 90% by PSD14 (Figure 6G, quantified in Figure S9) to its intact stage (Figure S6L). These data demonstrated that a massive pruning event was underway.

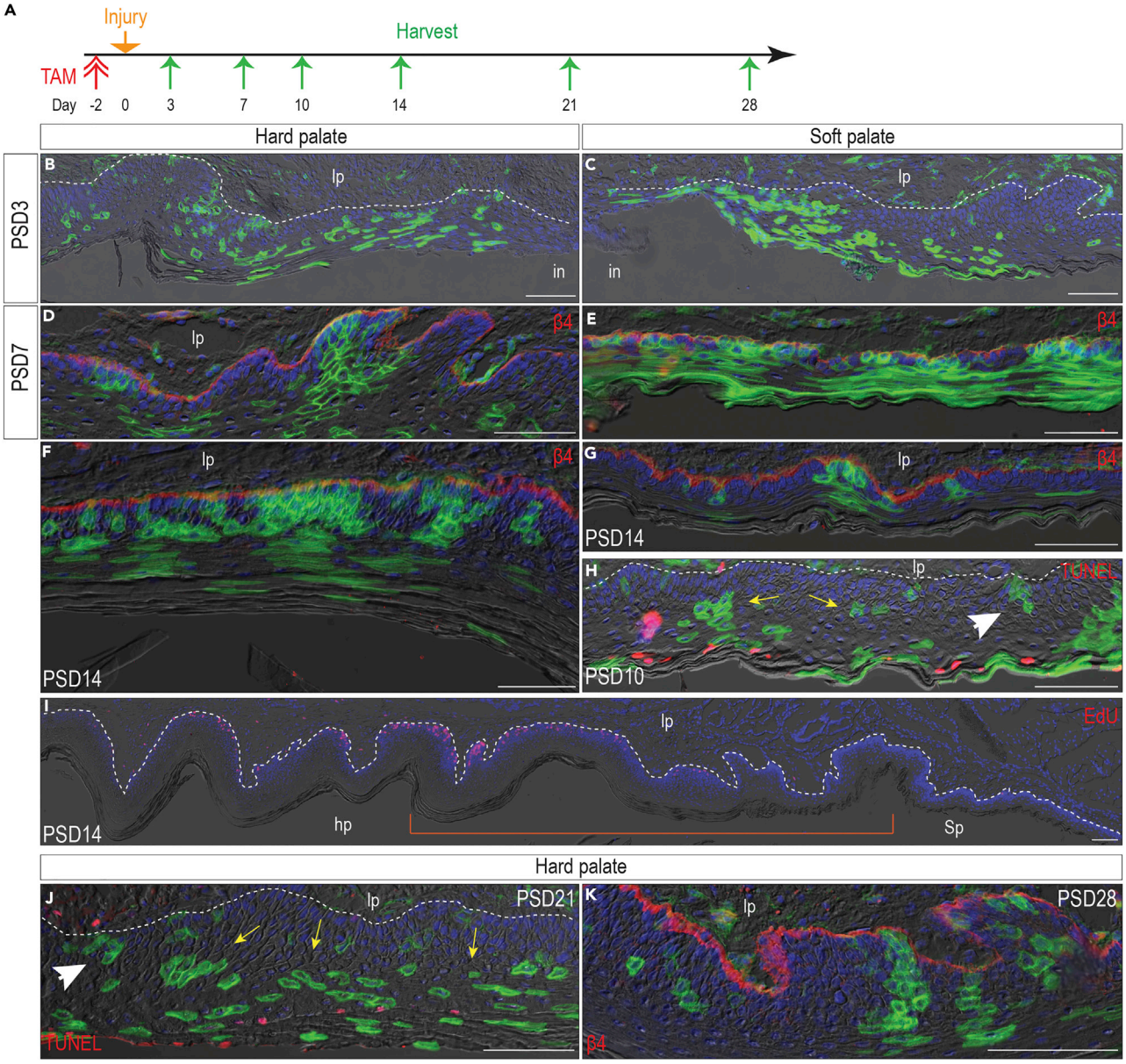

Figure 6. Wnt-Responsive Population Enlarges in Response to Proliferation but Prunes after Homeostasis Is Reestablished

(A) A schematic diagram showing the lineage tracing strategy. Mice were injected with one dose of tamoxifen at the age of 3 months. Two days later, a 2-mm full-thickness injury was generated in the hard and soft palates. Wnt-responsive cells were analyzed 3D, 7D, 10D, 14D, and 21D after surgery.

(B-C) On PSD3, GFP^{+ve} Wnt-responsive cells were examined in the healing (B) hard palate and (C) soft palate.

(D-E) On PSD7, GFP^{+ve} Wnt-responsive cells were examined in the healed (D) hard palate and (E) soft palate.

(F) On PSD14, abundant GFP^{+ve} Wnt-responsive cells still existed in the healed hard palate.

(G) By PSD14, GFP^{+ve} Wnt-responsive cells were returned to normal level.

(H) On PSD10, TUNEL were co-stained with GFP^{+ve} Wnt-responsive cells in the soft palate.

(I) EdU staining showing the proliferation of cells in both hard and soft palates on PSD14. Orange bracket indicates the injury site.

(J) On PSD21, TUNEL were co-stained with GFP^{+ve} Wnt-responsive cells in the hard palate.

(K) GFP^{+ve} Wnt-responsive cells in the hard palate 28D after injury. Wnt-responsive cells (green) were co-immunostained with β4 integrin (β4, red, basement membrane). Yellow arrows indicate Wnt-responsive cells in suprabasal layers. White arrowhead indicates Wnt-responsive cells in basal layer. Abbreviation: lp, lamia proper; hp, hard palate; sp, soft palate; PSD, post-surgery day. Scale bars: 100 μm.

See also Figures S5–S9.

Although the reduction in GFP^{+ve} epithelial clone size could be attributed to a higher level of turnover in the regenerated tissue, this would not explain the drastic reduction in GFP^{+ve} cells in the basal layer (from 85% to 17%, Figures 6E and 6G, quantified in Figure S9). We wondered if the GFP^{+ve} basal cells were undergoing apoptosis to re-establish homeostasis. Staining on PSD10 revealed only sporadic TUNEL^{+ve} cells, and none of them were in the basal layer (Figure 6H) as they were observed in the intact state (Figure S8). Thus, the pruning of Wnt-responsive basal cells was apparently fulfilled by halting self-renewal.

The same sequence of events also occurred in the hard palate, just at later time points: for example, on PSD14, when abundant Wnt-responsive cells were still present in the hard palate (Figure 5G), and cell proliferation remained high (Figure 6I), indicating the tissue remodeling was ongoing. On PSD21, most GFP^{+ve} cells were in suprabasal layers (Figure 6J) and homeostasis was ultimately re-established on PSD28 (Figure 6K, compared with Figure S6M).

Taken together, these data demonstrated that a stem population of GFP^{+ve} Wnt-responsive cells residing in the basal layer dramatically expanded in response to injury. Part of the response was to re-establish a stem cell pool in the new basal layer overlying the wound, and another part of the response was to then directly differentiate and regenerate the missing tissue. Thereafter, through mechanisms that do not appear to involve apoptosis, the stem cell pool was pruned back to the level seen during homeostasis.

DISCUSSION

Here, we report that Wnt-responsive basal cells in the hard and soft palates have a self-renewing capacity, give rise to differentiated suprabasal cells, and participate in tissue homeostasis and tissue regeneration. The hard and soft palates share similar homeostatic mechanisms and comparable injury responses; the main difference is that Wnt-responsive cells in the soft palate are more mitotically active, which correlates with a superior healing outcome.

To put these behaviors of oral epithelial stem cells in context, we considered other types of epithelial tissue. For several decades, researchers have characterized stem cells and described their self-renewing and differentiation capacities in skin. Multiple stem cell populations have been identified that contribute to both homeostasis and injury repair (Dekoninck and Blanpain, 2019). In comparison with skin, relatively little is known about stem cell populations in the oral mucosa. Mitotically active, long-lived BMI1^{+ve} oral mucosal progenitor cells in the basal layer of the lining mucosa participate in homeostasis (Jones et al., 2019). Selective cell ablation leads to expansion of BMI1^{+ve} clones, but their overall contribution to injury repair remains elusive (Jones et al., 2019). In our study, the Axin2^{+ve} population in the basal layer of the oral mucosa is also long-lived. This Axin2^{+ve} population maintains oral mucosa homeostasis (Figure 2), is activated by injury, and directly contributes to the regenerated tissue (Figures 4, 5, and 6). These similarities suggest that the two populations may overlap. In fact, several studies have linked BMI1 activity with Wnt signaling. BMI encodes a ring finger protein in the polycomb group complex that controls chromatin remodeling (Cho et al., 2013; Li et al., 2018), and at least one study shows that BMI1 promotes Wnt signaling in epithelial cells and cancer cells, perhaps through repressing the Wnt antagonist, Dickkopf (Cho et al., 2013; Li et al., 2018). Activating Wnt signaling via over-expression of Wnt1 promotes BMI1 expression as well (Cho et al., 2013). In ongoing studies, we are exploring the extent to which the Axin2^{+ve} Wnt-responsive population of stem cells overlaps with the BMI1^{+ve} population.

In our study, we also noticed that the number of Wnt-responsive basal cells is tightly controlled. During homeostasis, Wnt-responsive basal cells increased in a very slow rate (Figure 2). In response to injury, however, abundant new cells are required to quickly close a wound. We demonstrated that, during the repair process, Wnt-responsive cells produced ample progeny (Figure 6). These cells initially occupied a large percentage of the basal layer in the newly formed oral epithelia, but this state was transient. Shortly after re-epithelialization was complete, the percentage of Wnt-responsive basal cells was reduced (Figure 5) by halting their self-renewing capacity (Figure 6). We speculate that this "pruning" process represents a potential cancer-preventing mechanism based on the undisputed link between chronic injury and oncogenic transformation of the oral mucosa. We demonstrated that a stem cell population exists in the basal layer (Figure 2) and this stem cell population dramatically expands in response to injury (Figure 4). Most cancers arise from the accumulation of DNA mutations due to infidelity of the DNA replication and failure of DNA repair (Behrens et al., 2014; Vassilev and DePamphilis, 2017) and the risk of a stem cell undergoing oncogenic transformation is strongly correlated with the total number of divisions it undergoes (Tomasetti and

Vogelstein, 2015). Statistically, the chance that a random mutation arises during the rapid proliferation process in our model is high. If cells with such DNA mutations are not eliminated, they can initiate carcinogenesis (Batlle and Clevers, 2017; Lin et al., 2008). Currently, it is unclear how the body selects Wnt-responsive cells to stay in the basal layers as well as what the pruning mechanism is.

In our study, we examined the healing in both the hard and soft palate. Our data demonstrated that Wnt-responsive cells in the soft palate response to the injury more quickly (Figures 4 and 5). The hard palate and the soft palate are distinctive in their morphology (Figure 1) and, therefore, cells in these two tissues are in different mechanical environments. For example, the hard palate is exposed to compressive and shear forces during the mastication of food (Nanci, 2017) and the junction between its epithelium and underlying connective tissue is convoluted, to prevent the epithelium from detaching under shear force. The soft palate, on the other hand, is flexible and has a loose layer of elastic fibers underneath (Nanci, 2017). Tissue damage alters the mechanical environment of cells (Begnaud et al., 2016; Ladoux and Mege, 2017; Rousselle et al., 2018), and stem cells translate a change in the mechanical environment into molecular signals that activate cellular functions related to tissue repair. For example, changes in mechanical forces stimulate stem cell proliferation (Elbediwy et al., 2016; Vining and Mooney, 2017). We hypothesize that the robust cell proliferation that characterizes soft palate healing (Figure 4) may be activated by wound contracture and changes in extracellular matrix stiffness as part of the repair process (Li et al., 2014). One molecular pathway that is implicated in regulating stem cell function is the Hippo pathway, which integrates cytoskeletal changes in stem cells with alterations in the extracellular environment (Varelas, 2014; Zhao et al., 2011) during both tissue homeostasis and repair (Elbediwy et al., 2016). Whether TAZ/YAP also serves as a mechano-sensor/damage-sensor in oral mucosa is a focus of future studies.

Limitations of the Study

Although this study provided insights into the stem cell function of Wnt-responsive cells in oral epithelia, subsequent studies are necessary to demonstrate whether these cells are indispensable to maintain tissue integrity and support repair. One approach may be to ablate Axin2^{+ve} cells in epithelia, then study how the homeostasis and repair response is affected. It is also worth noting that we did not investigate the source of Wnt, neither during homeostasis nor during injury repair. Identifying the Wnt-secreting cells might help to understand the mechanism of the "trimming process" we observed after repair.

METHODS

All methods can be found in the accompanying Transparent Methods supplemental file.

SUPPLEMENTAL INFORMATION

Supplemental Information can be found online at https://doi.org/10.1016/j.isci.2019.10.016.

ACKNOWLEDGMENT

We thank Christina Mac, Ryan Ma, and Peter Chew for their assistance in cell culture, tissue processing, and staining. The study was funded by NIH grant R01DE024000-14 to J.A.H. and K99DE028585-01 to X.Y.

AUTHOR CONTRIBUTIONS

Conceptualization, X.Y. and J.A.H.; Methodology, X.Y., Q.X, X.Z, and J.A.H.; Investigation, X.Y., Q.X, X.Z, L.A.v.B., P.T., and J.A.H.; Writing – Original Draft, X.Y. and J.A.H.; Writing – Review & Editing X.Y., L.A.v.B., P.T., and J.A.H.; Funding Acquisition, X.Y. and J.A.H.; Resources, J.A.H.; Supervision, X.Y. and J.A.H.

DECLARATION OF INTERESTS

J.A.H. is an employee of Ankasa Regenerative Therapeutics, a biopharmaceutical company developing L-WNT3A for commercial use. The authors declare no competing financial interests.

Received: June 21, 2019
Revised: September 12, 2019
Accepted: October 4, 2019
Published: November 22, 2019

REFERENCES

Aragona, M., Dekoninck, S., Rulands, S., Lenglez, S., Mascre, G., Simons, B.D., and Blanpain, C. (2017). Defining stem cell dynamics and migration during wound healing in mouse skin epidermis. Nat. Commun. *8*, 14684.

Batlle, E., and Clevers, H. (2017). Cancer stem cells revisited. Nat. Med. *23*, 1124–1134.

Begnaud, S., Chen, T., Delacour, D., Mege, R.M., and Ladoux, B. (2016). Mechanics of epithelial tissues during gap closure. Curr. Opin. Cell Biol. *42*, 52–62.

Behrens, A., van Deursen, J.M., Rudolph, K.L., and Schumacher, B. (2014). Impact of genomic damage and ageing on stem cell function. Nat. Cell Biol. *16*, 201–207.

Bowman, A.N., van Amerongen, R., Palmer, T.D., and Nusse, R. (2013). Lineage tracing with Axin2 reveals distinct developmental and adult populations of Wnt/beta-catenin-responsive neural stem cells. Proc. Natl. Acad. Sci. U S A *110*, 7324–7329.

Cho, J.H., Dimri, M., and Dimri, G.P. (2013). A positive feedback loop regulates the expression of polycomb group protein BMI1 via WNT signaling pathway. J. Biol. Chem. *288*, 3406–3418.

Clevers, H., Loh, K.M., and Nusse, R. (2014). Stem cell signaling. An integral program for tissue renewal and regeneration: Wnt signaling and stem cell control. Science *346*, 1248012.

Dekoninck, S., and Blanpain, C. (2019). Stem cell dynamics, migration and plasticity during wound healing. Nat. Cell Biol. *21*, 18–24.

Elbediwy, A., Vincent-Mistiaen, Z.I., and Thompson, B.J. (2016). YAP and TAZ in epithelial stem cells: a sensor for cell polarity, mechanical forces and tissue damage. Bioessays *38*, 644–653.

Iglesias-Bartolome, R., Uchiyama, A., Molinolo, A.A., Abusleme, L., Brooks, S.R., Callejas-Valera, J.L., Edwards, D., Doci, C., Asselin-Labat, M.L., Onaitis, M.W., et al. (2018). Transcriptional signature primes human oral mucosa for rapid wound healing. Sci. Transl. Med. *10*, https://doi.org/10.1126/scitranslmed.aap8798.

Jones, K.B., Furukawa, S., Marangoni, P., Ma, H., Pinkard, H., D'Urso, R., Zilionis, R., Klein, A.M., and Klein, O.D. (2019). Quantitative clonal analysis and single-cell transcriptomics reveal division kinetics, hierarchy, and fate of oral epithelial progenitor cells. Cell Stem Cell *24*, 183–192.e8.

Jones, K.B., and Klein, O.D. (2013). Oral epithelial stem cells in tissue maintenance and disease: the first steps in a long journey. Int. J. Oral Sci. *5*, 121–129.

Kretzschmar, K., and Clevers, H. (2017). Wnt/beta-catenin signaling in adult mammalian epithelial stem cells. Dev. Biol. *428*, 273–282.

Ladoux, B., and Mege, R.M. (2017). Mechanobiology of collective cell behaviours. Nat. Rev. Mol. Cell Biol. *18*, 743–757.

Li, J., Johnson, C.A., Smith, A.A., Shi, B., Brunski, J.B., and Helms, J.A. (2014). Molecular mechanisms underlying skeletal growth arrest by cutaneous scarring. Bone *66*, 223–231.

Li, X.G., Wang, Z., Chen, R.Q., Fu, H.L., Gao, C.Q., Yan, H.C., Xing, G.X., and Wang, X.Q. (2018). LGR5 and BMI1 increase pig intestinal epithelial cell proliferation by stimulating WNT/beta-Catenin signaling. Int. J. Mol. Sci. *19* (4), 1036.

Lien, W.H., and Fuchs, E. (2014). Wnt some lose some: transcriptional governance of stem cells by Wnt/beta-catenin signaling. Genes Dev. *28*, 1517–1532.

Lin, E.H., Jiang, Y., Deng, Y., Lapsiwala, R., Lin, T., and Blau, C.A. (2008). Cancer stem cells, endothelial progenitors, and mesenchymal stem cells: "seed and soil" theory revisited. Gastrointest. Cancer Res. *2*, 169–174.

Nanci, A. (2017). Ten Cate's Oral Histology-E-Book: Development, Structure, and Function (Elsevier Health Sciences).

Politis, C., Schoenaers, J., Jacobs, R., and Agbaje, J.O. (2016). Wound healing problems in the mouth. Front. Physiol. *7*, 507.

Rousselle, P., Braye, F., and Dayan, G. (2018). Re-epithelialization of adult skin wounds: cellular mechanisms and therapeutic strategies. Adv. Drug Deliv. Rev. in press.

Squier, C.A., and Kremer, M.J. (2001). Biology of oral mucosa and esophagus. J. Natl. Cancer Inst. Monogr. 7–15.

Tomasetti, C., and Vogelstein, B. (2015). Variation in cancer risk among tissues can be explained by the number of stem cell divisions. Science *347*, 78–81.

van Amerongen, R., Bowman, A.N., and Nusse, R. (2012). Developmental stage and time dictate the fate of Wnt/beta-catenin-responsive stem cells in the mammary gland. Cell Stem Cell *11*, 387–400.

Varelas, X. (2014). The Hippo pathway effectors TAZ and YAP in development, homeostasis and disease. Development *141*, 1614–1626.

Vassilev, A., and DePamphilis, M.L. (2017). Links between DNA replication, stem cells and cancer. Genes *8*, 45.

Vining, K.H., and Mooney, D.J. (2017). Mechanical forces direct stem cell behaviour in development and regeneration. Nat. Rev. Mol. Cell Biol. *18*, 728–742.

Wang, B., Zhao, L., Fish, M., Logan, C.Y., and Nusse, R. (2015). Self-renewing diploid Axin2(+) cells fuel homeostatic renewal of the liver. Nature *524*, 180–185.

Winning, T.A., and Townsend, G.C. (2000). Oral mucosal embryology and histology. Clin. Dermatol. *18*, 499–511.

Yuan, X., Pei, X., Zhao, Y., Li, Z., Chen, C.H., Tulu, U.S., Liu, B., Van Brunt, L.A., Brunski, J.B., and Helms, J.A. (2018a). Biomechanics of immediate postextraction implant osseointegration. J. Dent Res. *97*, 987–994.

Yuan, X., Pei, X., Zhao, Y., Tulu, U.S., Liu, B., and Helms, J.A. (2018b). A Wnt-responsive PDL population effectuates extraction socket healing. J. Dent Res. *97*, 803–809.

Zhao, B., Tumaneng, K., and Guan, K.L. (2011). The Hippo pathway in organ size control, tissue regeneration and stem cell self-renewal. Nat. Cell Biol. *13*, 877–883.

ISCI, Volume *21*

Supplemental Information

Wnt-Responsive Stem Cell Fates in the Oral Mucosa

Xue Yuan, Quanchen Xu, Xiaohui Zhang, Lauren A. Van Brunt, Pavla Ticha, and Jill A. Helms

Supplemental figures and figure legends

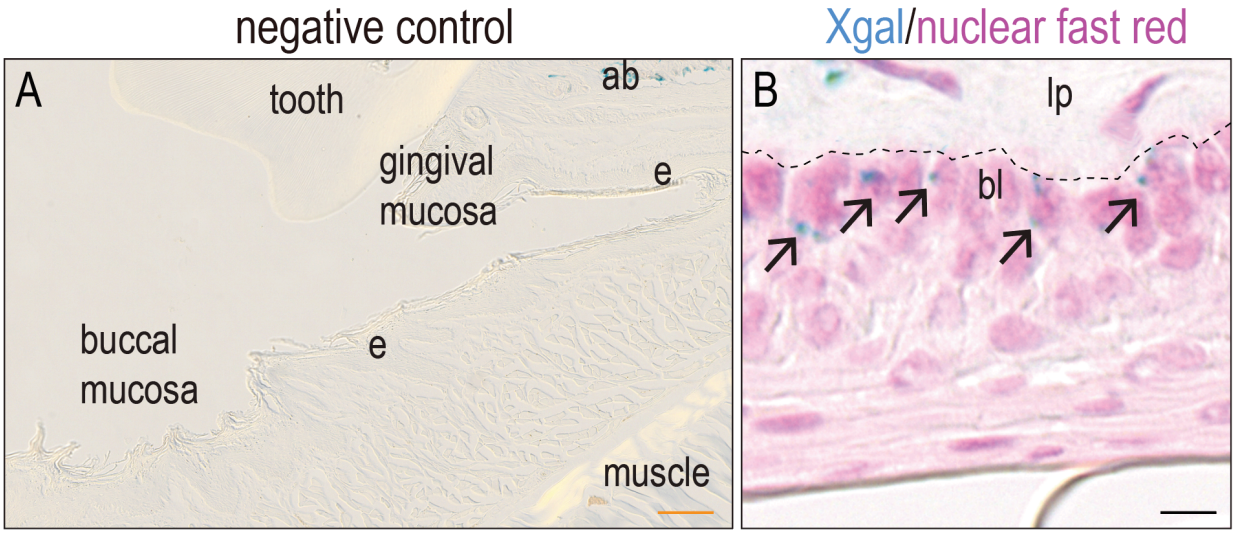

Figure S1. Xgal staining in the oral mucosa. Related to Figure 1. (A) A negative control of Xgal staining in the oral cavity. The section is from the *Axin2*$^{+/+}$ mouse. Non-specific Xgal staining was not evidence in the epithelial layer. Only the alveolar bone area showed non-specific signaling, which is known as osteoclasts. (B) Xgal co-stained with nuclear fast red. Nuclear fast red staining was used to distinguish the epithelial layer from the lamina propria. The dotted line indicates the basement membrane. Arrows indicate the Xgal^{+ve} cells. Abbreviations: ab, alveolar bone; e, epithelial layer; lp, lamina propria, bl, basal layer. Scale bars: orange = 100 μm; black = 10 μm.

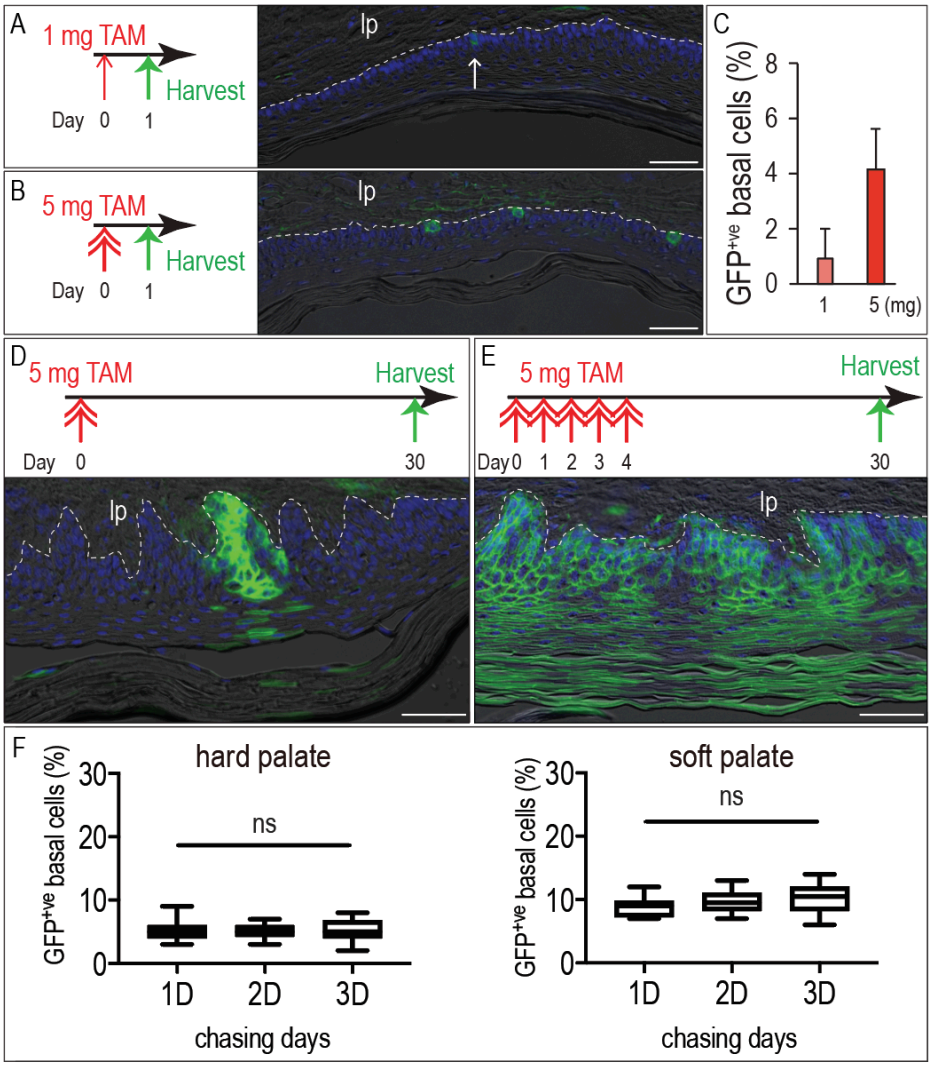

Figure S2. Titration of tamoxifen. Related to Figures 2 and 6. (A) GFP^{+ve} cells in the oral epithelium 1 day (D) after 1mg/25g body weight tamoxifen injection. Arrow indicates the GFP^{+ve} cell. (B) GFP^{+ve} cells in the oral epithelium 1D after 5mg/25g body weight tamoxifen injection. (C) Quantification of GFP^{+ve} basal cells in both groups. (D) GFP^{+ve} cells in the oral epithelium 30D after one-time 5mg/25g body weight tamoxifen injection. (E) GFP^{+ve} cells in the oral epithelium 30D after five-time 5mg/25g body weight tamoxifen injection. This label strategy resulted in a near-complete labeling of all cells in the oral mucosa, which made it impossible to follow the fate of a single clone. (F) Mice were injected with one-time 5mg/25g body weight tamoxifen and the GFP^{+ve} basal cells were quantified on 1D, 2D and 3D chasing from both hard palate and soft palate (n=3, 5 sections per mouse). The GFP^{+ve} basal cells remained the same from 1D to 3D in both tissues, indicating tamoxifen was below the threshold to activate Cre recombination 1D after the injection. Abbreviations: lp, lamina propria; TAM, tamoxifen. Scale bars: 50 μm. Data represent mean ± SD. ns: no significant difference as determined by one-way ANOVA, followed by Tukey's post hoc testing.

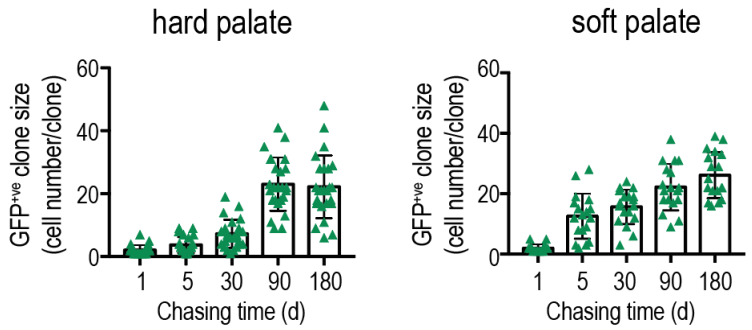

Figure S3. Quantification of GFP^{+ve} cell number in each clone in (A) the hard and (B) soft palates. Related to Figure 2. n=3, 5 sections for each mouse. Data represent mean ± SD.

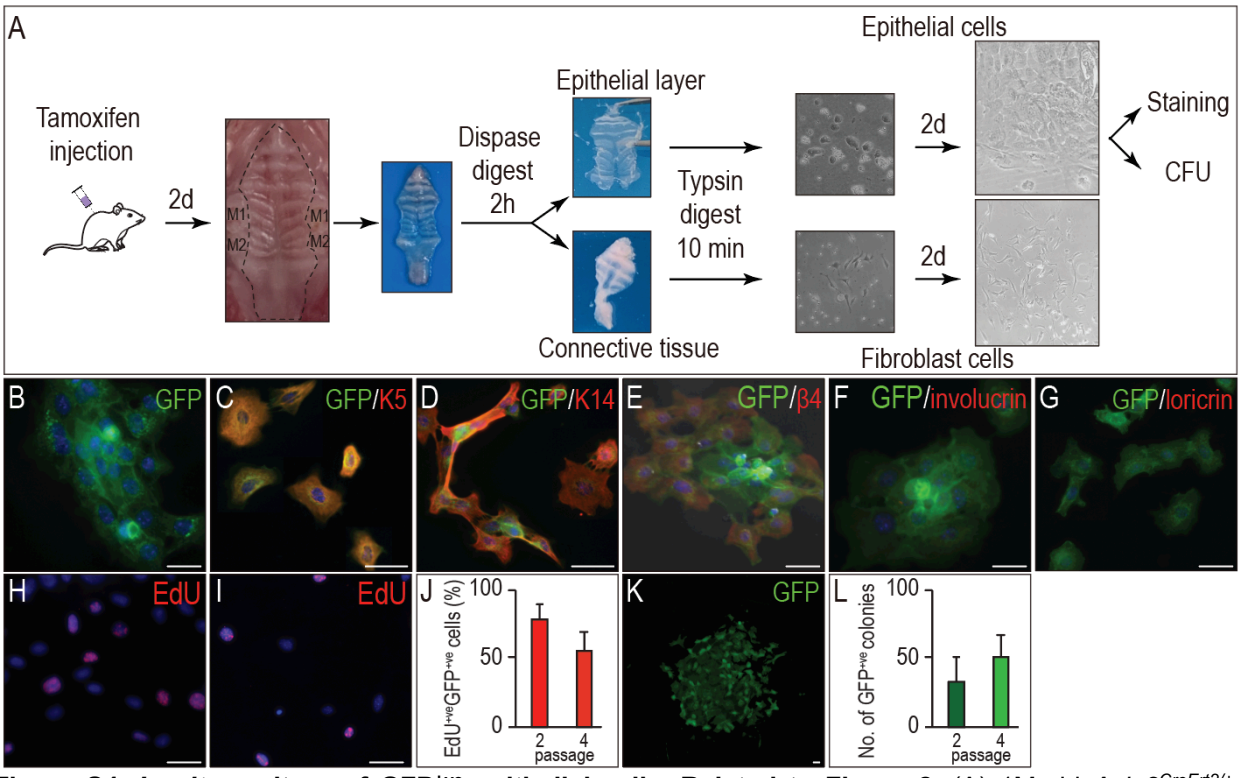

Figure S4. *In vitro* culture of GFP^{+ve} epithelial cells. Related to Figure 2. (A) 1M-old *Axin2$^{CreErt2/+}$; R26$^{mTmG/+}$* mice received tamoxifen two days before sacrifice. The hard and soft palates were isolated and digested with dispase for two hours. After digestion, the epithelial layer and the connective tissue were separated and then digested with trypsin for 10 min. The epithelial cells and the fibroblasts were cultured in plates. The epithelial cells were split once and then subjected for staining and colony-forming unit (CFU) assay. (B) GFP^{+ve} epithelial cells. GFP^{+ve} cells were co-stained with (C) keratin 5, (D) keratin 14, (E) integrin β4, (F) involucrin, (G) loricrin. EdU staining for the GFP^{+ve} cells in (H) 2nd passage and (I) 4th passage. (J) Quantification of the EdU^{+ve} cells. (K) GFP^{+ve} colony in 4th passage. (L) Quantification of colony formed by GFP^{+ve} cells. Scale bars: 25 μm. Data represent mean ± SD.

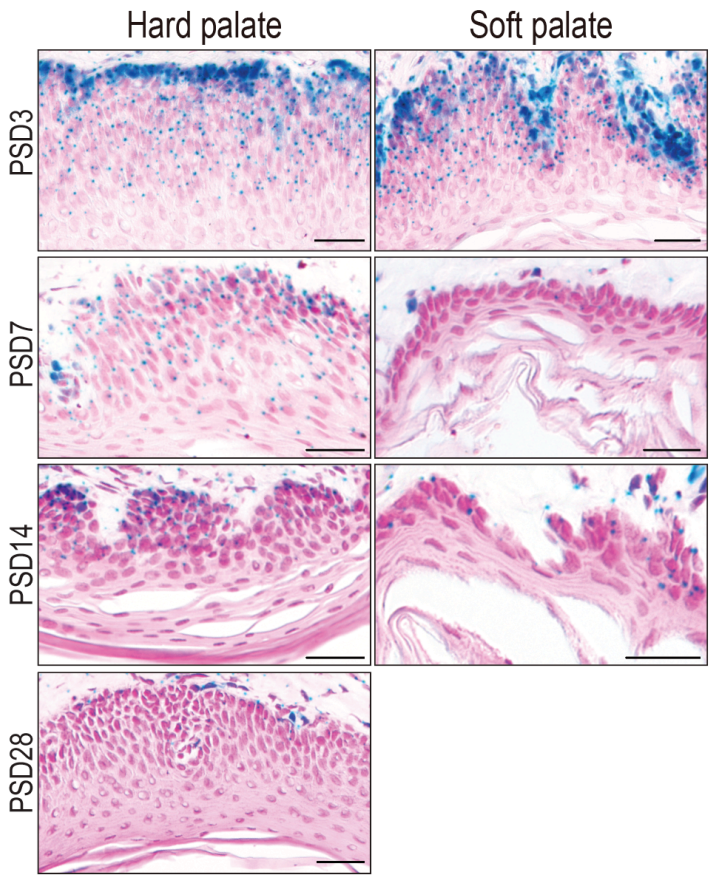

Figure S5. Xgal co-stained with nuclear fast red. Related to Figures 4 and 5. Scale bars: 50 μm.

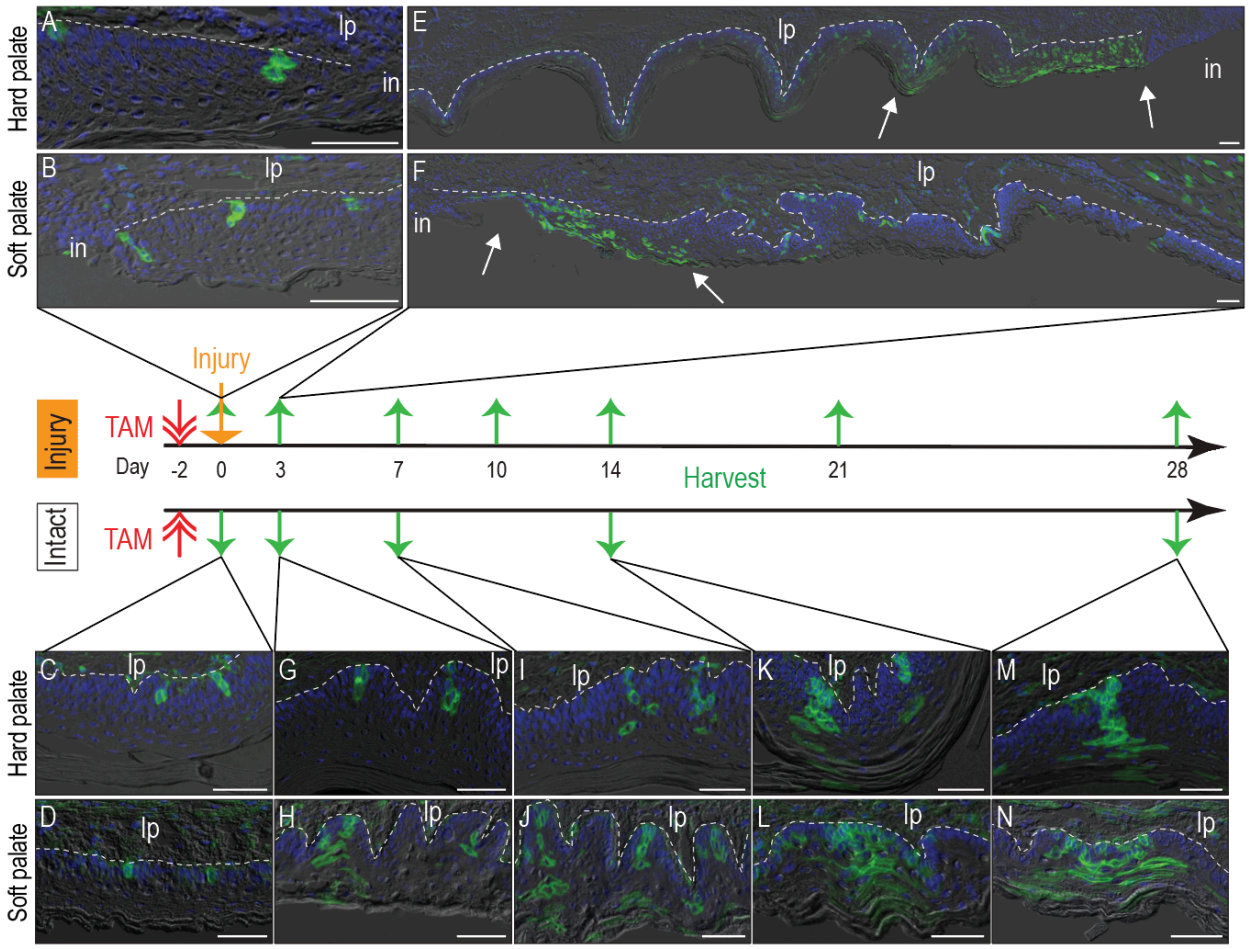

Figure S6. Lineage tracing of GFP^{+ve} Wnt-responsive cells. Related to Figure 6. A schematic diagram showing the lineage tracing strategy. Mice were injected with one-dose of tamoxifen at the age of 3M. For the injury group, a 2 mm full-thickness injury was generated 2D after tamoxifen injection. Wnt-responsive cells were analyzed immediately, 3D, 7D, 10D, 14D and 21D after surgery. After injury (PSD0), GFP^{+ve} Wnt-responsive cells were examined in the remaining (A) hard palate and (B) soft palate. GFP^{+ve} Wnt-responsive cells were also examined in the intact (C) hard palate and (D) soft palate at the same time point. On PSD3, GFP^{+ve} Wnt-responsive cells were examined in the remaining (E) hard palate and (F) soft palate. GFP^{+ve} Wnt-responsive cells were accumulated in the edge as indicated by arrows. Wnt-responsive cells were also examined in the intact (G) hard palate and (H) soft palate at the same time point. For injury group, Wnt-responsive cells on PSD7, 10, 14, 21, and 28 are showing in Figure 6. For the same time point controls, Wnt-responsive cells were shown in I-N. Abbreviations: lp, lamina propria; in, injury. Scale bars: 50 μm.

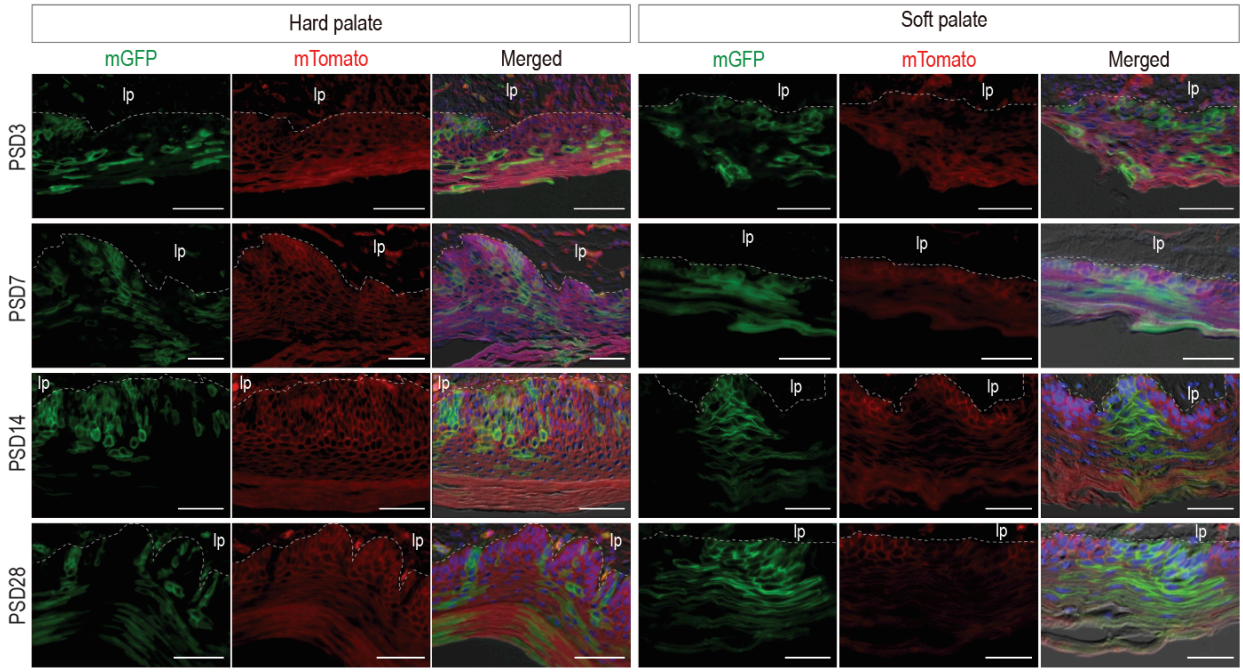

Figure S7. Lineage tracing of Wnt-responsive cells 3D, 7D, 10D, 14D and 28D after injury. Related to Figure 6. In *Axin2*$^{CreERT2/+}$*; R26R*$^{mTmG/+}$ mice, all cells express cell membrane-localized tdTomato (mTomato, red). Cre recombinase expressing cells, which require the present of Wnt signaling and tamoxifen at the same time, have cell membrane localized EGFP (mGFP, green) fluorescence expression replacing the mTomato. Future cell lineages derived from these cells are still positive for mGFP. The dotted line indicates the basement membrane. Abbreviations: lp, lamina propria. Scale bars: 50 μm.

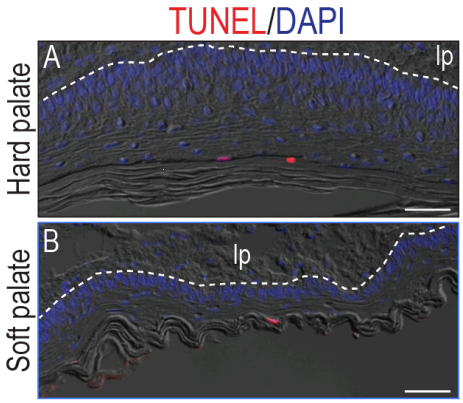

Figure S8. TUNEL staining of intact (A) hard and (B) soft palates. Related to Figure 6. The dotted line indicates the basement membrane. Abbreviations: lp, lamina propria. Scale bars: 50 μm.

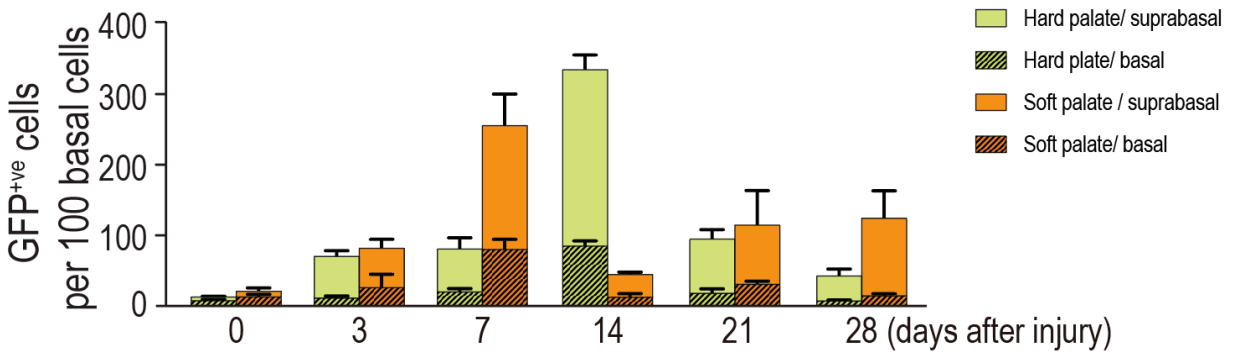

Figure S9. Quantification of GFP^{+ve} cells. Related to Figure 6. For quantification, a region of interest is defined as 100 μm (~100 cells) from the edge of the injury (PSD0) or 200 μm from the center of the injury (PSD3, 7, 14, 21, and 28) for both hard and soft palates. Basal cells were defined as cells that colocalized with the β4 integrin. n=3, 5 sections per mouse. Data represent mean ± SD.

Transparent Methods

Animals

All experimental protocols followed the ARRIVE (Animal Research: Reporting of In Vivo Experiments) guidelines and were approved by the Stanford Committee on Animal Research (#13146), which is an AAALAC-accredited animal care and use program. *Axin2*$^{CreERT2/+}$*; R26R*$^{mTmG/+}$ mice (#018867 and #007576) and *Axin2*$^{LacZ/+}$ mice (#11809809) were purchased from Jackson Laboratories (Bar Harbor, ME, USA) and housed in a temperature-controlled environment with 12-hour light/dark cycles. All experiments were conducted using both genders. Age of analyzed mice is indicated in each figure legend.

Lineage tracing

Tamoxifen (T5648, Sigma) was dissolved in ethanol first and then diluted with sunflower seed oil to the final concentration of 10 mg/ml. The frequency of Cre recombination was affected by tamoxifen dosage. To find the proper concentration for lineage tracing, we initially tested tamoxifen of 1mg/25g body weight and 5mg/25g body weight. We also tested one injection versus five injections. Analyses of the resulting patterns of GFP^{+ve} supported the conclusion: a one-time, 5mg/25g body weight dose of tamoxifen resulted in GFP^{+ve} colonies that were sufficient to be detectable yet isolated enough to allow separation of each colony (Figure S2). Therefore, in this study, we delivered tamoxifen as a single injection of 5mg/25g body weight.
3-month old *Axin2*$^{CreERT2/+}$*; R26R*$^{mTmG/+}$ mice were used for lineage tracing and mice were sacrificed at indicated time points.

Surgeries

3-month old *Axin2*$^{CreERT2/+}$*; R26R*$^{mTmG/+}$ mice were given tamoxifen before injury to label the existing Wnt-responsive cells. The mice received same dose of tamoxifen but without any injury were used as control. Two days after tamoxifen injection, mice were anesthetized with Ketamine and Xylazine, followed by subcutaneous injections of buprenorphine. A 2 mm full-thickness injury was generated with a biopsy punch (Miltex, Inc., USA). The wound was in the junction: half of the injury in the hard palate and the other half in the soft palate (Figures 3A and 3B). Bleeding was controlled by local pressure. After surgery, mice were supplied with a soft diet for one week.

Sample preparation, histology and cellular assays (Masson's trichrome staining, Movet's Pentachrome staining, Xgal staining, immunohistochemistry staining)

Maxillae were harvested and fixed with 4% paraformaldehyde (PFA) overnight at 4°C. Following 10-day decalcification with 10% ethylenediaminetetraacetic acid (EDTA), specimens were incubated with 30% sucrose in phosphate-buffered saline (PBS) overnight and then embedded with Tissue-Tek OCT embedding medium. Tissues were cut into 8 μm-thick sections and collected on Superfrost-plus slides.
To visualize the morphology of oral mucosa, we performed a Masson's trichrome staining with the staining kit from Electron Microscopy Sciences (#26367) according to the manufacturer's instruction. Movat's pentachrome staining was also performed (Arioka et al., 2019), in which nuclei stain blue to black, cytoplasm stains red, collagen stains yellow to greenish yellow, and fibrous tissue stains an intense red (Movat, 1955).
To detect β-galactosidase activity, we performed an Xgal staining with a staining solution containing 5 mM potassium ferricyanide, 5 mM potassium ferrocyanide, 2 mM $MgCl_2$, and 1 mg/ml Xgal (Thermo Fisher Scientific). Sections were rinsed with PBS, dehydrated with a graded ethanol series, cleared in CitriSolv, and then mounted with Permount (Chai et al., 2000; Kim et al., 2007). For quantification, the sections were stained with nuclear fast red (N3020, Sigma-Aldrich). In *Axin2*$^{LacZ/+}$ mice, Xgal^{+ve} signaling is restricted to the nuclei in Wnt-responsive cells (appeared punctate staining) because of the NLS (nuclear localization signal)-LacZ. To address the possibility that Xgal staining was non-specific, we included a negative control, e.g., *Axin2*$^{+/+}$ littermates that carry no LacZ gene (Zhang et al., 2019). Tissues from these mice were fixed, processed and stained side-by-side with *Axin2*$^{LacZ/+}$ samples. Non-specific staining was only found in the alveolar bone area (Figure S1A) as has been reported previously (Odgren et al., 2006).
Immunostaining was performed as described before (Minear et al., 2010) with slight modifications. In brief, tissue sections were permeabilized with 0.5% Triton X-100 and blocked with R.T.U. Animal-Free Block and Diluent (SP-5035, Vector Laboratories) for 30 min. Samples were incubated with β4 integrin (Clone 346-11A, BD science) antibody or β-catenin (ab6302, Abcam) antibody overnight at 4°C. After washing with PBS, slides were incubated with Cyanine 5 conjugated goat anti-rat secondary antibody (Invitrogen, A10525) or Cyanine 5 conjugated goat anti-rabbit secondary antibody (Invitrogen, A10523) for 30 min, then mounted with ProLong™ Gold Antifade Mountant with DAPI (Thermo Fisher Scientific).

Cell proliferation and apoptosis

EdU incorporation assay was used to examine cell proliferation. Cell proliferation is characterized by DNA replication. 5-ethynyl-2'-deoxyuridine (EdU), a thymidine analog, is readily incorporated into DNA during DNA synthesis. Incorporated EdU can be detected by a fluorescent azide through a Cu(I)-catalyzed [3 + 2] cycloaddition reaction (''click'' chemistry) (Salic and Mitchison, 2008). Mice were injected intraperitoneally with EdU (50 mg/kg) in PBS and harvested 2 hours later. Samples were fixed and processed as described above. Tissues were permeabilized with 0.5% Triton X-100. Click-iT reaction cocktail was prepared with EdU in vivo kits (BCK-IV-IM, Base Click, Germany) according to the protocol and was applied to each section for 30 min. The slides were then washed and mounted with ProLong™ Gold Antifade Mountant with DAPI (Thermo Fisher).

Terminal deoxynucleotidyl transferase dUTP nick end labeling (TUNEL) staining was used to detect cell apoptosis. The assay was performed with Click-iT Plus TUNEL assay for In Situ Apoptosis Detection kit (C10619, Thermo Fisher) according to the manufacturer's instruction.

Primary cultures of GFP^{+ve} oral epithelial cells

1-month old *Axin2$^{CreERT2/+}$; R26R$^{mTmG/+}$* mice (both males and females) were given tamoxifen 2 days before sacrifice. Oral epithelial cells were isolated as described (Igarashi et al., 2008; Nakamura et al., 2003) with some modifications. In brief, the hard and soft palates were peeled off from the palatal bone and then incubated with 2.4 IU dispase II (Roche, Indianapolis, IN) at 37℃ for 2 h with shaking. After separating the epithelial layer with the connective tissue, both parts were subjected to trypLE Express (ThermoFisher Scientific) digest for 10 min to dissociate cells. The cells were cultured in DMEM (ThermoFisher Scientific) + 10% FBS and maintained in a humidified atmosphere of 5% CO2 at 37℃ (Figure S4A). Plates for epithelial cell culture were coated with type I collagen (10 μg/cm^2, C3867, Sigma).

Immunofluorescence was performed with following primary antibodies: keratin 5 (905504, Biolegend), keratin 14 (905301, Biolegend), β4 integrin (Clone 346-11A, BD science), involucrin (924401, Biolegend), and loricrin (ab24722, Abcam). Cyanine 5 conjugated goat anti-rat antibody (Invitrogen, A10525) or Cyanine 5 conjugated goat anti-rabbit antibody (Invitrogen, A10523) was used as secondary antibodies.

To access the cell proliferation ability, EdU was added to the culture media as a final concentration of 100 μM for 2 hours. The cells were then washed, fixed and performed Click-iT reaction (BCK-IV-IM, Base Click, Germany).

In order to evaluate colony forming efficiency, 1x10^4 cells were seeded on collagen coated 100 mm dish. After 14 days, cells were fixed and imaged. GFP^{+ve} colonies with more than 20 cells were counted (n=3).

Quantification and statistical analyses

To quantify GFP^{+ve} cells, GFP was co-stained with β4 integrin. GFP^{+ve}β4 integrin^{+ve} cells were defined as GFP^{+ve} basal cells. GFP^{+ve}β4 integrin^{-} cells were defined as GFP^{+ve} suprabasal cells. DAPI^{+ve} β4 integrin^{+ve} cells were counted and used as basal cell number. The result was expressed as the number of GFP^{+ve} basal cells or GFP^{+ve} suprabasal cells per 100 basal cells. Each time point included at least 3 mice, and 5 slides from each mouse at each time point were calculated.

To quantify Xgal^{+ve} cells, Xgal was co-stained with nuclear fast red (Figure S1B). The epithelial tissue can be easily distinguished from the connective tissue from its unique cell morphology and higher cell density. The first layer of epithelial cells that facing the connective tissue was defined as the basal layer. Xgal^{+ve} cells and total cells in basal layer were counted. The result was expressed as the number of Xgal^{+ve} cells per 100 basal cells. Each time point included at least 3 mice, and 5 slides from each mouse at each time point were calculated.

For injury response, each time point included at least 6 mice. A region of interest is defined as 1 mm (~100 cells) from the edge of the injury (PSD0) or 2 mm from the center of the injury (PSD3, 7, 14, 21, and 28) for both hard and soft palates. To quantify the wound healing, wound areas in the hard and soft palates were calculated by Image J. The results were expressed as the percentage of the remaining open wound area over the total original wound area (n=6). The repair rate was calculated based on the histology images from PSD1 and PSD3. For each sample, only sections close to the middle line were selected and the length of the repaired hard and soft palates were measured by Image J. The repair rate was expressed as the length of the newly formed tissue (mm) per day (n=6). EdU^{+ve} basal cells in the hard and soft palates were calculated using the same method described above for GFP^{+ve} cells.

Results are presented as the mean ± standard deviation of independent replicates (n≥3). Comparison was based on a one-way ANOVA, followed by Tukey's post hoc testing. P≤0.05 was considered significant. The program GraphPad Prism (GraphPad Software, Inc., San Diego, USA) was used for these analyses.

Supplemental References:

Arioka, M., Zhang, X., Li, Z., Tulu, U.S., Liu, Y., Wang, L., Yuan, X., and Helms, J.A. (2019). Osteoporotic Changes in the Periodontium Impair Alveolar Bone Healing. J Dent Res *98*, 450-458.

Chai, Y., Jiang, X., Ito, Y., Bringas, P., Jr., Han, J., Rowitch, D.H., Soriano, P., McMahon, A.P., and Sucov, H.M. (2000). Fate of the mammalian cranial neural crest during tooth and mandibular morphogenesis. Development *127*, 1671-1679.

Igarashi, T., Shimmura, S., Yoshida, S., Tonogi, M., Shinozaki, N., and Yamane, G.Y. (2008). Isolation of oral epithelial progenitors using collagen IV. Oral Dis *14*, 413-418.

Kim, J.B., Leucht, P., Lam, K., Luppen, C., Ten Berge, D., Nusse, R., and Helms, J.A. (2007). Bone regeneration is regulated by wnt signaling. J Bone Miner Res *22*, 1913-1923.

Minear, S., Leucht, P., Jiang, J., Liu, B., Zeng, A., Fuerer, C., Nusse, R., and Helms, J.A. (2010). Wnt proteins promote bone regeneration. Science translational medicine *2*, 29ra30.

Movat, H.Z. (1955). Demonstration of All Connective Tissue Elements in a Single Section - Pentachrome Stains. Arch Pathol *60*, 289-295.

Nakamura, T., Endo, K., Cooper, L.J., Fullwood, N.J., Tanifuji, N., Tsuzuki, M., Koizumi, N., Inatomi, T., Sano, Y., and Kinoshita, S. (2003). The successful culture and autologous transplantation of rabbit oral mucosal epithelial cells on amniotic membrane. Invest Ophthalmol Vis Sci *44*, 106-116.

Odgren, P.R., MacKay, C.A., Mason-Savas, A., Yang, M., Mailhot, G., and Birnbaum, M.J. (2006). False-positive beta-galactosidase staining in osteoclasts by endogenous enzyme: studies in neonatal and month-old wild-type mice. Connect Tissue Res *47*, 229-234.

Salic, A., and Mitchison, T.J. (2008). A chemical method for fast and sensitive detection of DNA synthesis in vivo. Proc Natl Acad Sci U S A *105*, 2415-2420.

Zhang, X., Yuan, X., Xu, Q., Arioka, M., Van Brunt, L.A., Shi, Y., Brunski, J., and Helms, J.A. (2019). Molecular Basis for Periodontal Ligament Adaptation to In Vivo Loading. J Dent Res *98*, 331-338.